J|A|C|S
ARTICLES
Published on Web 02/14/2002

# Size-Dependent Melting of Silica-Encapsulated Gold Nanoparticles

Kimberly Dick, T. Dhanasekaran, Zhenyuan Zhang, and Dan Meisel*

*Contribution from the Radiation Laboratory and Department of Chemistry and Biochemistry, University of Notre Dame, Notre Dame, Indiana 46556*

Received October 11, 2001. Revised Manuscript Received December 12, 2001

***Abstract:*** We report on the size dependence of the melting temperature of silica-encapsulated gold nanoparticles. The melting point was determined using differential thermal analysis (DTA) coupled to thermal gravimetric analysis (TGA) techniques. The small gold particles, with sizes ranging from 1.5 to 20 nm, were synthesized using radiolytic and chemical reduction procedures and then coated with porous silica shells to isolate the particles from one another. The resulting silica-encapsulated gold particles show clear melting endotherms in the DTA scan with no accompanying weight loss of the material in the TGA examination. The silica shell acts as a nanocrucible for the melting gold with little effect on the melting temperature itself, even though the analytical procedure destroys the particles once they melt. Phenomenological thermodynamic predictions of the size dependence of the melting point of gold agree with the experimental observation. Implications of these observations to the self-diffusion coefficient of gold in the nanoparticles are discussed, especially as they relate to the spontaneous alloying of core−shell bimetallic particles.

## Introduction

The physical properties of small particles are a subject of intense contemporary interest. As the size decreases to the nanometer scale, many of the electronic, as well as the thermodynamic, properties are significantly altered from those of either the bulk or the single molecule. In the present report, we focus on the effect of size on melting temperature of $SiO_2$-encapsulated small gold nanoparticles. Depression of the melting point of small particles below that of the bulk, when the dimensions approach a few nanometers, has been known for a long time. This dependence of melting on size is not restricted to any particular material; rather, it encompasses a wide variety of materials from metals to semiconductors and to molecular organic crystals.[1−7] A recent rare observation of melting point of tin clusters above the melting of the bulk is taken to indicate a structure different for the clusters from the bulk.[8] Theoretical phenomenological considerations, based on the classical Kelvin equation, led Pawlow nearly a century ago to develop a quantitative relationship between the melting temperature, $T_m$, and the particle size.[9] Whereas this correlation is not quantitatively accurate, it still is often utilized to estimate the size dependence of $T_m$. For a particle of diameter $d$ and molar heat of fusion $L$, the Pawlow relation is given in eq 1:

$$\frac{T_m(r)}{T_m(\infty)} = 1 - \frac{4v_s^{2/3}}{L}(\gamma_s 2v_s^{2/3} - \gamma_l 2v_l^{2/3})\frac{1}{d} \qquad (1)$$

where $v$ and $\gamma$ are the specific molar volume and surface free energy of the solid (s) and liquid (l), respectively, and $\infty$ signifies the bulk material. Later theoretical treatments improved the agreement with experimental determinations, but they all predict the inverse dependence on diameter, similar to eq 1.[2,7,10−12]

A thorough systematic experimental study of the size-dependent melting of gold nanoparticles was carried out by Buffat and Borel using electron diffraction techniques compared with several other techniques.[6] Their version of the modified Pawlow relation, eq 2

$$\frac{T_m(r)}{T_m(\infty)} = 1 - \frac{4}{\rho_S L}\left\{\gamma_s - \gamma_l\left(\frac{\rho_S}{\rho_l}\right)^{2/3}\right\}\frac{1}{d} \qquad (2)$$

gives a very good description of the experimental observations.[6,7] The symbols in eq 2 have the same meaning as those in eq 1. This equation is also used in this study to compare the present results with earlier observations, and it was recently evoked to rationalize morphology control of small gold particles.[13,14]

Several other studies, experimental and theoretical, of the size dependence of the melting temperature of metals find similar

(1) Sheng, H. W.; Lu, K.; Ma, E. *Nanostruct. Mater.* **1998**, *10*, 865.
(2) Sambles, J. R. *Proc. R. Soc. London, Ser. A* **1971**, *324*, 339.
(3) Peters, K. F.; Cohen, J. B.; Chung, Y.-W. *Phys. Rev. B* **1998**, *57*, 13430.
(4) Goldstein, A. N.; Echer, C. M.; Alivisatos, A. P. *Science* **1992**, *256*, 1425.
(5) Cleveland, C. L.; Luedtke, W. D.; Landman, U. *Phys. Rev. B* **1999**, *60*, 5065.
(6) Buffat, P.; Borel, J.-P. *Phys. Rev. A* **1976**, *13*, 2287.
(7) Borel, J.-P. *Surf. Sci.* **1981**, *106*, 1.
(8) Shvartsburg, A. A.; Jarrold, M. F. *Phys. Rev. Lett.* **2000**, *85*, 2530.
(9) Pawlow, P. *Z. Phys. Chem.* **1909**, *65*, 545.
(10) Hoshino, K.; Shimamura, S. *Philos. Mag. A* **1979**, *40*, 137.
(11) Hasegawa, M.; Hoshino, K.; Watabe, M. *J. Phys. F: Met. Phys.* **1980**, *10*, 619.
(12) Sambles, J. R.; Skinner, L. M.; Lidgarten, N. D. *Proc. R. Soc. London, Ser. A* **1970**, *507*, 318.
(13) Maye, M. M.; Zheng, W.; Leibowitz, F. L.; Ly, N. K.; Zhong, C. J. *Langmuir* **2000**, *16*, 490.
(14) Maye, M. M.; Zhong, C.-J. *J. Mater. Chem.* **2000**, *10*, 1895.



**10.1021/ja017281a CCC: $22.00** 

strong dependence on size.[1,3,8,15,16] The experimental techniques require highly specialized instrumentation and elaborate analysis both in the generation of the particles and in the determination of the melting point. We report here on a simple approach to determine the dependence of the melting temperature of gold nanoparticles encapsulated in silica shells on size. Wet colloidal chemistry techniques were used to generate well-defined particles of relatively narrow size distribution and encapsulate them in silica. Silica has a higher melting point than gold and, therefore, does not interfere with the temperature measurement.

Our interest in the melting of the particles at lowered temperatures is triggered by recent reports on laser-induced melting of mono- and bimetallic nanoparticles.[17−20] These studies provide a detailed kinetic description of the process of melting focusing on the fast time regime that leads to equilibration of the electronic excitation with lattice phonons. The present report provides a rationale for the suggestion that the small particles generated by these techniques do not necessarily maintain their solid integrity at ambient temperature for a long time. At the size of a few nanometers, metallic particles might become liquid, possibly labeled as droplets, even if their bulk metal temperature is hundreds of degrees higher. This implies that even if composite particles are originally constructed as core−shell structures they may spontaneously alloy at relatively low temperatures and over relatively short periods of times.[21] Furthermore, even when the original core−shell structure can be convincingly demonstrated for the larger sizes, the potential for easy alloying at ambient temperature needs to be considered as the size decreases.

Well-documented reduction methods were used in this study to prepare the gold nanoparticles from their parent ions. The first follows the well-known Turkevich procedure, where citrate ions reduce gold at moderately elevated temperature.[22,23] The second technique adapts the methodology developed by Henglein and co-workers using radiolytically generated organic free radicals, which in turn reduce the gold salt.[20,24,25] The gold nanoparticles obtained using this strategy are narrowly dispersed high-quality particles, which are not easy to obtain by other techniques. The gold nanoparticles were then coated with a shell of silica to isolate them from one another, following the procedure of Liz-Marzan et al.[26] This step was necessary to avoid coalescence of the small particles as the temperature is raised. It also enhances the chemical stability of the small particles that are extremely sensitive to oxygen. Once encapsulated, the particles can be precipitated and filtered out of the suspension without oxidation and aggregation of the metallic particles. The melting temperature of the resulting powder of silica-encapsulated particles was directly determined using differential thermal analysis (DTA) coupled to thermal gravimetric analysis (TGA). This gives a simple, direct, and clear illustration of the melting temperature of the powder of the colloidal particles. We find, in agreement with earlier determinations of vapor deposited gold particles and with earlier theoretical predictions, that the melting point strongly depends on particle sizes below 5 nm. It is also concluded that the silica shell has only a small effect on the melting point of the gold core, presumably because of the high porosity of the shell. Quantitatively, though, the melting temperature is somewhat higher than that observed by Buffat and Borel, presumably because of the enhanced stability obtained by the shell.[6]

## Experimental Section

**Preparation of Colloidal Gold Nanoparticles.** The largest particles in this study (15 nm particle diameter) were produced using the Turkevich method of reduction and stabilization by citrate.[22,23] The smallest particles (1.5−2.5 nm) were produced by radiolysis,[25] and the midsized particles were produced using radiolytic enlargement of the smaller particles.[24] Briefly, the Turkevich method involves the reduction of a gold salt to metallic colloidal gold by citrate at moderately high temperatures. First, 0.2 g of $H[AuCl_4]\cdot 3H_2O$ dissolved in 200 mL of water was added to 800 mL of boiling water, for a final gold concentration of $5.0 \times 10^{-4}$ M. When the solution returned to a boil, 100 mL of 1% weight of sodium citrate solution was added. This solution was boiled for approximately 20 min, until the solution attained a deep wine red color indicating the formation of colloidal gold nanoparticles.

For the smallest particles, 50 mL of aqueous $2.0 \times 10^{-4}$ M $NaAuCl_4\cdot 3H_2O$ and 0.5 M methanol solution was prepared in an airtight vessel. The size of the particles produced was determined by the stabilizer used. The smallest particles (1.5 nm) were stabilized with $1.0 \times 10^{-3}$ M sodium citrate, while the 2.5 nm particles were stabilized with 0.01 M poly(vinyl alcohol) (PVA).[25,27] These solutions were deaerated for 15 min and then irradiated for 8 min at $1.2 \times 10^6$ rad/h in a $^{60}Co$ $\gamma$-source. Finally, the small suspended "seed" particles were enlarged by combining one part seed solution with seven parts of a solution containing $2.0 \times 10^{-4}$ M $KAu(CN)_2$, 0.5 M methanol, and $1.0 \times 10^{-4}$ M sodium citrate as a stabilizer. This combination of concentrations nominally enlarges the particles to twice their original diameter. The resulting solution was bubbled with $N_2O$ gas for 5 min, then irradiated at $2.2 \times 10^5$ rad/h for 60−90 min, until the absorbance of the gold particles in the plasmon-band range remained unchanged. The enlarged particles were in turn further enlarged to twice their diameter by the same procedure as above, irradiating 3−6 h until no change in the plasmon band was observed. The particles produced in these procedures were characterized by transmission electron microscopy (TEM). For particles of sizes larger than 2 nm the size distribution was narrower than ±10%. It was significantly broader (up to ±20%) for smaller sizes.

**Encapsulation and Precipitation.** Immediately after preparation of the gold suspensions, the precursor solutions for coating with silica shells were added to the gold suspensions.[26,28] First, the bifunctional linker molecule 3-aminopropyltrimethoxysilane (APS) was added as a primer, in an amount just sufficient to form one monolayer on the particles. The cross section of an APS molecule was assumed to be 40 Å$^2$. The combined solution of linker and sol was stirred for one-half of an hour, and then an excess of sodium silicate solution, 3 times the mass of the gold, was added. The sols were allowed to stir for 2−3 days, until no change in the visible spectra occurred. Following encapsulation, high concentrations of sodium chloride were added and the suspension diluted to twice its original volume with neat ethanol, inducing coagulation of the nanoparticles out of the suspension. Once the nanoparticles settled, the liquid was decanted, and the precipitate

(15) Ross, J.; Andres, R. P. *Surf. Sci.* **1981**, *106*, 11.
(16) Shimizu, Y.; Sawada, S.; Ikeda, K. S. *Eur. Phys. J. D* **1998**, *4*, 365.
(17) Fujiwara, H.; Yanagida, S.; Kamat, P. V. *J. Phys. Chem. B* **1999**, *103*, 2589.
(18) Link, S.; Wang, Z. L.; El-Sayed, M. A. *J. Phys. Chem. B* **2000**, *104*, 7867.
(19) Link, S.; Wang, Z. L.; El-Sayed, M. A. *J. Phys. Chem. B* **1999**, *103*, 3529.
(20) Hodak, J. H.; Henglein, A.; Giersig, M.; Hartland, G. V. *J. Phys. Chem. B* **2000**, *104*, 11708.
(21) Shibata, T.; Tostmann, H.; Bunker, B.; Henglein, A.; Meisel, D.; Cheong, S.; Boyanov, M. *J. Synchrotron Radiat.* **2001**, *8*, 545.
(22) Enustun, B. V.; Turkevich, J. *J. Am. Chem. Soc.* **1963**, *85*, 3317.
(23) Turkevich, J.; Stevenson, P. C.; Hillier, J. *Discuss. Faraday Soc.* **1951**, *11*, 55.
(24) Henglein, A.; Meisel, D. *Langmuir* **1998**, *14*, 7392.
(25) Henglein, A. *Langmuir* **1999**, *15*, 6738.
(26) Liz-Marzan, L. M.; Giersig, M.; Mulvaney, P. *Langmuir* **1996**, *12*, 4329.
(27) Henglein, A.; Giersig, M. *J. Phys. Chem. B* **1999**, *103*, 9533.
(28) Makarova, O. V.; Ostafin, A. E.; Miyoshi, H.; Norris, J. R.; Meisel, D. *J. Phys. Chem. B* **1999**, *103*, 9080.

was washed and filtered using an ultrafiltration membrane (MW 10 000) in a pressurized chamber. The precipitate was then washed with excess water to remove the sodium chloride unless otherwise noted. Yet, traces of sodium chloride did appear in the DTA melting experiments, especially for the smaller size particles, but were easily recognizable. For the largest particles studied, this procedure generates shells of ~5 nm thickness. It was difficult to discern the core boundaries in the TEM micrographs of the smaller particles. Because the gold to silica concentrations ratio was maintained constant throughout the preparations, the shell thickness decreases upon decreasing the core size.

**Melting Temperature Experiments.** The melting temperatures of dried powders of the particles were determined using the DTA and TGA techniques simultaneously. A computer-controlled SDT-2960 DTA-TGA apparatus from TA Instruments was used, and each sample was scanned from room temperature to 1100 °C, above the melting point of bulk gold. In these experiments, very small samples (5−30 mg) were placed under helium inside a sealed chamber, and their weight and temperature were monitored closely with thermocouples situated under the sample and the reference. Alumina was used as the reference material in these experiments. The chamber was heated at a rate of 20 °C per minute, and the temperature and mass of both the sample and the reference were monitored at all times, to an accuracy of $1 \times 10^{-3}$ °C and $1 \times 10^{-4}$ mg, respectively. Any phase transition or chemical change in the sample requires absorption or release of a small amount of energy. Since the energy input is constant, the heating rate of the sample relative to the reference will momentarily decrease or increase as this change takes place. The first derivative of the temperature difference between the sample and the reference was recorded to offset systematic differences in the rate of heating the sample relative to the reference and enhance the appearance of any phase transition. It should be noted that since alumina conducts slightly better than silica, the sample temperature, measured at the bottom of the sample, lags behind the temperature of the reference. This leads to a constant slope in the DTA plots. The derivative of this plot effectively normalizes the constant sloping baseline.

**Control Experiments.** Several control experiments were conducted to determine possible interference with the melting temperature measurements. Samples of uncoated gold particles, hollow silica shells, and PVA were all measured. For the "naked" gold colloid, the "as-synthesized" particles were filtered out and dried by ultrafiltration. As mentioned above, without the silica coating, the smaller size nanoparticles are unstable. They are easily oxidized and coagulate. Therefore, these control experiments were performed only for gold particles of size ≥5 nm. Melting temperatures of coagulated and precipitated large gold particles also provided an accurate calibration of our DTA instrument. We obtain, in agreement with literature values, a melting temperature of $T_m(\infty) = 1064$ °C for the largest particles used. This temperature did not change upon repeated temperature cycling, despite visible changes in appearance of the gold following the first melting, indicating that at that size bulk melting is attained.

For the control sample that contains silica alone, gold particles were prepared again by the Turkevich method, and silica coating was grown on them as described above. The particles were precipitated and washed to obtain a solid powder. Subsequently, they were resuspended in 50 mL of water under vigorous stirring. This effectively lowered the pH of the sample from around 9.0 to nearly neutral. Then, 0.1 M NaCN was added to the sample to dissolve the gold core from within the silica shells. The metallic particles are thus oxidized to $Au(CN)_2^-$ ions, and the silica shells remain suspended in the solution. They were eventually precipitated and dried prior to the temperature measurement. Flakes of the PVA polymer that was used to stabilize the nanoparticles were also checked for their effect in the DTA experiments in their original form.

## Results and Discussion

**Production, Enlargement, and Encapsulation of the Au Particle.** The radiolytic method for the production of gold particles uses methanol radicals as the reductant[25]. The radiolysis of water produces free radicals that in turn produce methanol radicals, by the following sequence of reactions:

$$H_2O \rightsquigarrow e^-_{aq}, H, OH \quad (3)$$

$$e_{aq}^- + N_2O\ (+H_2O) \rightarrow N_2 + OH\ (+OH^-) \quad (4)$$

$$OH + CH_3OH \rightarrow H_2O + CH_2OH \quad (5)$$

$$H + CH_3OH \rightarrow H_2 + CH_2OH \quad (6)$$

The methanol radicals then reduce gold ions, producing metallic gold nanoparticles and formaldehyde.

$$3CH_2OH + Au(III) \rightarrow Au^0 + 3CH_2O + 3H^+ \quad (7)$$

H atoms, and $e^-_{aq}$ in the absence of nitrous oxide in solution, directly reduce gold ions also. The free energy required to reduce gold ions to individual gold atoms is much higher than the energy required to reduce the ions to gold atoms on a gold lattice. Therefore, following the initial formation of seed particles, most of the gold ions are reduced onto already-formed seeds. Consequently, the initial seeds tend to grow uniformly with little formation of new seeds. This results in gold particles of a relatively narrow size distribution. Larger size particles were produced by radiolytic enlargement of the particles produced by the above method.[24] To enlarge, $Au(CN)_2^-$ is added to the seed suspension, along with additional methanol and citrate, and the mixture is irradiated further. The cyanide complex is used because its redox potential is more negative than that of other Au(I) complexes, and methanol radicals cannot reduce the complex to individual atoms.[29] This ensures that all the gold is deposited on the preexisting seeds rather than producing new seeds. However, $e^-_{aq}$ does reduce $Au(CN)_2^-$ ions directly to produce the individual atoms. Therefore, all solutions containing $Au(CN)_2^-$ ions were saturated with nitrous oxide prior to irradiation. To attach silica to gold nanoparticles, APS is used as a primer. The amine headgroup conveniently binds to the particle surface, and the siloxane headgroup serves as a condensation nucleus for building the silica shell.

**DTA/TGA Analysis.** Figure 1 shows a representative first derivative DTA curve along with the corresponding TGA curve for 10 nm gold nanoparticles encapsulated in silica. Several observations are interesting to note. The large change at low temperatures is due to release of the water/ethanol mixture left in the sample. Although the nanoparticle powder was dried at room temperature, solvent molecules from the precipitation procedure remain entrapped in the porous silica matrix. Up to approximately 35% of the total powder weight could be lost in this step. This loss of solvent occurs near the boiling temperature of the water/ethanol azeotrope (78 °C), indicating that ethanol is the major component that remains in the silica pores despite its higher vapor pressure than that of water. In the temperature range of 250−300 °C, an irregular step is observed. This is attributed to pyrolysis of the organic stabilizer in the sample. It

(29) Mulvaney, P.; Giersig, M.; Henglein, A. *J. Phys. Chem.* **1993**, *97*, 7061.

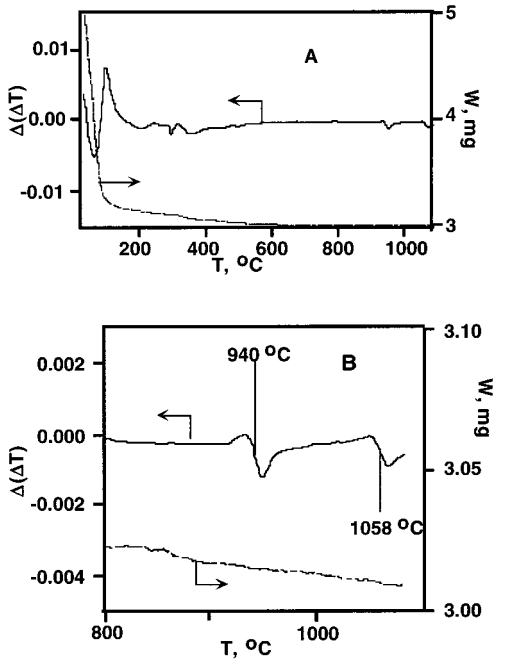


***Figure 1.*** (A) First derivative DTA (left-hand side scale) and TGA (right-hand side scale) profile of 10 nm silica-encapsulated gold particles. The large endotherm at ~80 °C is loss of the water/ethanol azeotrope, the one at 940 °C is melting of the particles, and the band at ~1060 °C is melting of bulk gold. (B) A detailed view of the gold-melting region.

could be observed in all of the samples, but the lowest melting point observed is higher than that pyrolysis band. For example, it appears as a shoulder on the low-temperature side of the melting endotherm of the smallest particles used (see Figure 3 below).

No further events can be observed in Figure 1 until the sample reaches a temperature of 940 °C, where a new endotherm can be seen. This latter event is not accompanied by any weight loss, as the TGA curve shows. Another small change is observed near 1060 °C (again no weight loss). This event is attributed to the well-established melting point of bulk gold (1064 °C). It was further verified by measuring the DTA of the as-prepared 15 nm gold nanoparticle stabilized by citrate but without any silica shell. The obtained dark blue coagulated powder showed only one very sharp endotherm in the DTA curve at 1064 °C without any corresponding change in the TGA curve. After cooling the sample, a shiny yellow solid of gold is obtained. In the absence of any physical barrier, the organic stabilizer pyrolyzes upon heating. The melting material forms bulk gold, ultimately melting again near 1064 °C. The endotherm in this case is more intense than that of the silica-encapsulated gold, presumably due to the larger weight fraction of gold in the sample in that case.

The melting endotherm at 1064 °C was observed in all samples studied regardless of particle size. This is attributed to the porosity of the silica, which allows flow of the melting gold to form large interconnected particles. This also indicates that the vapor pressure within the silica shell is maintained at atmospheric pressure. However, recycling the temperature for the second time on the same sample does not show the size-dependent melting endotherm again. The first-cycle melting destroys the identity of the small particles and leaves bulk material behind. None the less, all the observed changes are

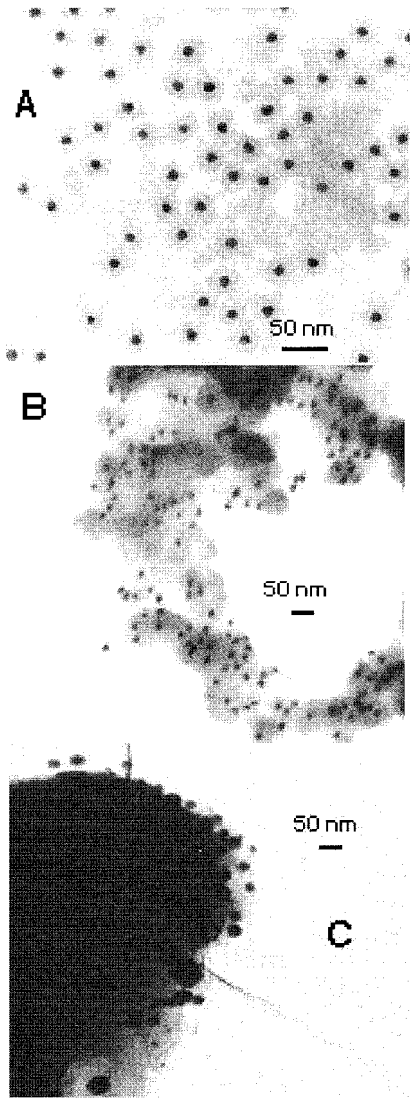


***Figure 2.*** TEM images of the silica-encapsulated 15 nm gold particles. (A) Deposited from the suspension directly onto the grid. (B) After induced coagulation and washing. (C) After cycling to 1100 °C.

highly reproducible with a fresh sample indicating irreversible changes to the material.

Electron microscopy supports this proposition. Figure 2 shows TEM images of 15 nm gold-core particles encapsulated in the silica shell. The particles deposited on the grid directly from the suspension (Figure 2a) show the well-defined gold core and silica shell. Most of the silica appears as shells around the gold core. None of the gold particles remains uncoated. Precipitation of the particles as described in the Experimental Section induces clumping of the silica, and most of the particles are now touching one another (Figure 2b). Yet, the gold cores are easily discernible. The core−shell structure is completely destroyed following the DTA temperature cycling, and the size of even the smallest particles is significantly increased (Figure 2c).

Figure 3 shows the first derivative DTA curve for the smallest particles used in this study, 1.5 nm gold core encapsulated in silica. All the previously noted endotherms can be seen in this sample as well. The melting of gold particles is observed here at 380 °C. In addition, a new endotherm appears in this experiment at ~805 °C, which was not observed in the samples of the larger particles. This peak is attributed to melting of the

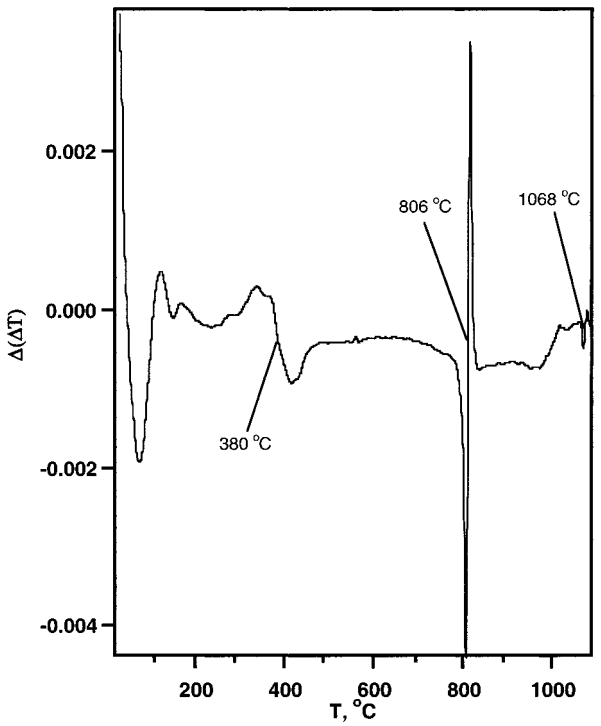


***Figure 3.*** First derivative DTA profile of 1.5 nm silica-encapsulated gold particles. The large endotherm at ~800 °C is melting of NaCl, the broad one at 380 °C is melting of the particles, and the band at 1068 °C is melting of bulk gold.

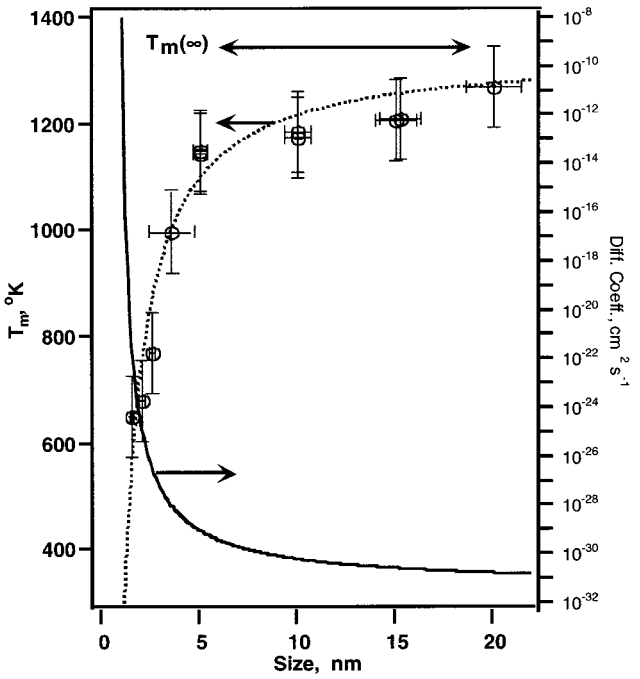


***Figure 4.*** Size dependence of the melting point and diffusion coefficient of silica-encapsulated gold particles. The dotted curve is calculated using eq 2 and the parameters given in the text for "naked" gold. The bulk melting temperature of Au is indicated by the double arrow as $T_m(\infty)$. The solid curve (right-hand side axis) is the calculated Au self-diffusion coefficient.

NaCl salt, which was used to induce coagulation of the silica-coated particles. Because of the sensitivity of the sample to air and because of the presence of the organic stabilizer, it is difficult to completely wash the salt out of the sample. The temperature of this band coincides with that of NaCl melting, and this region of temperatures does not interfere with the range of interest for the sample.

It is evident in the DTA profiles (e.g., Figure 3) that the width of endotherms is a function of the particle size, becoming broader with decreasing size. For comparison in Figure 3, the melting point of NaCl, and of the bulk gold, produces very narrow peaks, while the water/ethanol mixture produces a somewhat broader peak, due to deviations from ideal azeotropic composition. The melting endotherms for larger sizes of gold nanoparticles (5 nm and larger) are considerably sharper than those for the smaller particles. This indicates a broader distribution of melting temperatures within the samples, which increases with decreasing size. Indeed, the size distribution of the smaller particles is not as narrow as that of the larger ones. However, the primary reason for the broader melting temperature range is the extreme sensitivity of the melting point to the size in that region as is expected from eqs 1 and 2. A ±10% size distribution in the range of 2 nm corresponds to approximately ±200 °C in melting point distribution. The width of the endotherm for the smallest particle sizes in Figure 3 agrees well with the size distribution observed in the TEM determinations.

Figure 4 summarizes the size dependence of the melting point of the particles studied here. Even for particles of 20 nm the melting point is noticeably lower than that of the bulk. Using the parameters given by Buffat and Borel ($\rho_s$ and $\rho_l = 19$ and 17.3 g cm$^{-3}$ for the solid and liquid, respectively; $\gamma_s$ and $\gamma_l = 0.9 \times 10^3$ and $0.74 \times 10^3$ erg cm$^{-2}$, respectively; $L = 5.38 \times 10^8$ erg g$^{-1}$)[6] consistently yields higher melting temperatures than those experimentally observed. Fitting the experimental results to eq 2 and using the surface energy of the solid, $\gamma_s$, a quantity that is difficult to measure, as a variable parameter provides a best fit when $\gamma_s = 1000$ erg cm$^{-2}$. This value is well within the reported values for $\gamma_s$ for gold. The dashed curve in Figure 4 is calculated using eq 2 with these parameters. Large increases in surface tension parameter were noted earlier for Au, Pt,[31] and CdS[4] nanoparticles relative to the bulk values. The smaller difference in surface tension between the bulk and the nanoparticles may be attributed to the presence of the silica at the surface of the gold core. In the classical description of bare particles, this parameter should be independent of size.

We now turn to the implications of the lowered melting temperature. One of the consequences of this classical effect is expected to be an increase in the self-diffusion of the metal atoms. An approximate estimate of the self-diffusion coefficient, $D$, as a function of size is given in Figure 4. It was obtained assuming a Boltzmann−Arrhenius dependence of $D$ on temperature, eq 8:

$$D = D_o \exp(-\Delta H_d/kT) \tag{8}$$

where the activation enthalpy of diffusion is $\Delta H_d = 1.76$ eV for gold and the preexponential factor is $D_o = 0.04$ cm$^2$ s$^{-1}$.[30,31] Using eq 8, the bulk diffusion coefficient at room temperature is thus $2 \times 10^{-32}$ cm$^2$ s$^{-1}$, slow enough to eliminate any spontaneous diffusion from the surface to the bulk. Sharp phase boundaries might be expected, and indeed reported, for relatively large core−shell particles for extended periods of time.[20] At the melting point, 1337 K, the diffusion coefficient in the bulk

(30) Tu, K. N.; Mayer, J. W.; Feldman, L. C. *Electronic Thin Film Science*; Macmillan Publishing Co.: New York, 1992.
(31) Tyrrell, H. J. V.; Harris, K. R. *Diffusion in Liquids*; Butterworth: London, 1984.

can be calculated to be $D_m = 1 \times 10^{-8}$ cm$^2$ s$^{-1}$. Assuming $D_m$ is the same for all gold particles, independent of the melting temperature, and therefore independent of the size, one can then calculate the dependence of the diffusion coefficient at ambient temperature (or any other temperature) on the size, using eq 9:

$$D(\mathrm{r}) = D_m \exp[-\Delta H_d(\mathrm{r})(T^{-1} - T_m(\mathrm{r})^{-1})] \qquad (9)$$

The enthalpy of activation of diffusion is also expected to be size dependent as suggested in eq 9. In the calculation shown in Figure 4, it was assumed that $\Delta H_d(\mathrm{r})$ is proportional to the average number of bonds that needs to be broken in the melting process. This is a relatively small correction; in a particle of a fcc lattice, when all atoms that compose the particle are at the surface, assumed to be a 111 face, it amounts to 75% of $\Delta H_d$ of the bulk. The calculation shown in Figure 4 yields $D \approx 10^{-24}$ cm$^2$ s$^{-1}$ for a 2 nm particle at room temperature. This order of magnitude of diffusion coefficient will allow alloying of small particles on a time scale of days.[21] Preliminary results from our laboratory indeed indicate size-dependent alloying of the gold core into the silver shell and vice versa.[32]

(32) Shibata, T.; Zhang, Z.; Bunker, B.; Meisel, D., to be published.

## Conclusions

Silica coating of gold nanoparticles proves to be a very efficient approach to preserve the identity of the nanoparticles even at high temperatures. This is due to the stability of silica at high temperatures. DTA along with TGA examination provides a clear picture of the phase transitions that take place in the gold-silica nanocomposite. Because of the steep dependence of the melting temperature on size, this approach is highly dependent on the ability to narrow the size distribution of the particles and the ability to attach controlled silica shells to the metallic core. As a result of the depressed melting point in the small sizes, the metallic particle is much "softer" than the larger particles at ambient temperatures, leading to processes that are not expected for the bulk material. The increase in the diffusion coefficient may lead to spontaneous alloying of bimetallic particles,[32] and the same parameters are expected to offer control over the morphology of the particles, as indeed was recently reported.[13]

**Acknowledgment.** We thank Prof. Paul McGinn and Ms. H. Reichenbach for use of their DTA/TGA apparatus. Support by the U.S. Department of Energy, Office of Basic Energy Sciences, is gratefully acknowledged. This is contribution No. NDRL 4341 from the Notre Dame Radiation Laboratory.

JA017281A